Influencing Precision-Determining Weld Seam Properties in Laser Welding of Copper and Aluminum by Spatial Superposition of 445 nm and 1070 nm Wavelength Lasers

Christoph Spurk[1], Daniel Nettelbeck[2], André Häusler[3], Alexander Olowinsky[3], and Arnold Gillner[1]

[1]*RWTH Aachen University, Chair for Laser Technology LLT, Aachen, Germany*
[2]*FH Aachen - University of Applied Sciences, Aachen, Germany*
[3]*Fraunhofer Institute for Laser Technology ILT, Aachen, Germany*
[*]*Corresponding author's e-mail: christoph.spurk@llt.rwth-aachen.de*

For the contacting of battery cells, a stable and time-efficient joining process is required, whereas primarily copper and aluminum materials with high electrical conductivity are used. To ensure a high level of automation and process efficiency, laser micro welding has established itself in industrial applications. Single-mode fiber lasers in the near-infrared range with high brilliance offer the possibility of achieving high welding depths, although more than 90% of the initial laser power is lost due to reflection losses irradiating copper materials [1]. Laser beam sources in the blue emission spectrum, by contrast, have higher absorption in copper or aluminum, but cannot yet be focused to comparably small spot diameters in the required power range. To combine the advantages of both approaches, this paper follows the principle of spatial beam superposition of 445 nm and 1070 nm lasers, pursuing the goal of influencing precision-determining weld seam properties of copper and aluminum. This includes the formation of the melt pool, the consistency of the process regarding the welding depth and the influence on the surface roughness. As materials, Cu-ETP, CuSn6 and EN AW-6082 are analyzed to investigate the influence of different thermal conductivities on the process in addition to different base materials.
DOI: 10.2961/jlmn.2026.01.2012

Keywords: dual beam welding, blue laser radiation (445 nm), near-infrared laser radiation (1070 nm), copper, aluminum

1. Introduction

In Germany, the automotive industry is the most research-intensive sector and accounts for one third of all research investment. In the coming years, conventional technologies in the automotive industry will gradually be replaced by new trends. The automation of driving functions, the networking of individual vehicles with each other and with central points in the infrastructure, such as traffic lights or charging stations, and the electrification of vehicles will play an important role in this development [2]. A stable and time-efficient joining process is required for contacting battery cells or power electronics in battery-electric vehicles. Copper plays a central role here due to its good electrical conductivity. An average of 23 kilograms of copper is used in vehicles with combustion engines, whereas up to 83 kilograms are required in fully electric vehicles [3-4].

Laser beam micro welding has established itself as a high-quality process for contacting battery cells or power electronics due to its high degree of automatability and process efficiency. The contacting of copper materials using high-brilliance near-infrared laser beam sources offers the possibility of achieving weld depths with high aspect ratio, even though more than 90% of the initial laser power is reflected and is therefore not available for the joining process. The high power required to generate a deep welding process can result in a considerable proportion of the laser power being reflected, which can cause potential damage to surrounding components [1,5]. Laser beam sources in the visible wavelength regime show higher initial absorption in materials such as copper, iron, or gold. At a wavelength of $\lambda = 445$ nm, absorption is approximately 50%, which means that more energy is available for material processing. Furthermore, in copper or aluminum, absorption increases with rising temperature, both at wavelengths in the near-infrared range and at wavelengths in the visible range, thus complicating process quality and process control since more heat is introduced into the interaction zone. Inaccurate process control and resulting inconsistent energy input led to damage to components under the welded joints [3,5-7].

In material processing, new approaches are pursuing the combination of two beam sources. The targeted combination of highly focusable beam sources in the near-infrared wavelength regime and beam sources in the visible wavelength regime is intended to combine the advantages of both laser beam types. Investigations into laser micro welding with two wavelengths focus on the possibility of generating more melt volume and increasing the welding depth. Ensuring high precision in laser welding is a key challenge in industrial processes. This precision is crucial not only during the individual welding process, but also in terms of the repeatability of successive welding processes. When superimposing two laser beam sources, novel material-laser interactions are to be expected. Relevant evaluation criteria for laser beam welding include surface roughness and the consistency of

the weld seam width and penetration depth, as well as the repeatability of successive welding processes to ensure consistent quality assurance.

Based on the research topics of subproject A01 of the Collaborative Research Center SFB 1120 at RWTH Aachen University, this paper evaluates investigations of laser beam welding processes in which two laser beams with wavelengths of λ = 445 nm and 1070 nm are superimposed. The scientific focus addresses the consistency of the weld seam width and penetration depth, as well as the roughness of the generated weld seam. The laser beam emitted in the blue emission spectrum (λ = 445 nm) with a focal diameter of 609 µm remains stationary during the experiments and is superimposed with a dynamically controllable near-infrared (λ = 1070 nm) laser beam (NIR) with a focal diameter of 34 µm. The investigations are carried out at feed rates of 100 mm/s and the laser power of the individual sources is varied and adjusted according to the characteristic intensity threshold for achieving a deep penetration welding process. The materials are CuSn6, Cu-ETP and EN AW-6082. In addition, the focus point of the near-infrared laser is aligned coaxially, upstream and downstream to the focus point of the blue laser spot, where it is of interest whether the arrangement of the focus points has an observable influence on the results of the focus weld seam width, roughness, and welding depth. The results of the experiments are evaluated by cross and longitudinal sections of the weld samples, microscope images of the sections and the seam surface, and roughness measurements. Based on the theses measured variables and their results, the influence of the superimposed energy input on the welding results is to be investigated.

2. Theoretical Background

2.1. Single beam welding with different wavelengths

Laser beam welding is divided into two basic processes, heat conduction welding and deep penetration welding, where in heat conduction welding, the energy is mainly transferred from the material surface into the material by heat conduction [8,9]. The transition from heat conduction welding to deep penetration welding occurs when the energy input is increased and a threshold intensity is exceeded, causing the material-specific evaporation temperature to be reached. Within a generated vapor capillary, the laser beam can interact with the absorbing surfaces multiple times increasing energy coupling sharply. While the capillary stays in equilibrium with external forces, process fluctuations can occur because of pressure hotspots or inhomogeneous energy inputs [6,10].

The process quality and weld seam geometry depend largely on the geometry and stability of the vapor capillary. If the capillary is constricted induced by the fluctuations, a gas-filled bubble forms in the molten pool resulting in a pore in the weld seam. The geometry of the vapor capillary is not only shaped by the directly incident laser beam and its wavelength, but also by the interaction of the incident beam with the front of the vapor capillary itself. The reflected radiation in the vapor capillary depends on several process parameters, such as feed rate, focus diameter, wavelength, and power [6, 8, 11]. In addition to the vapor capillary, the flow in the molten pool, commonly referred to as the flow around the capillary, the metal vapor-induced flow and the Marangoni flow, are also relevant for the welding process. In experiments, the various effects of the individual flow principles cannot be clearly separated from one another. However, an estimate can be made depending on the feed rate, where for low feed rates (< 200 mm/s), metal vapor-induced flow and Marangoni flow are responsible for the melt pool dynamic [8,12].

Regarding process control, laser beam welding also allows the use of temporal and spatial power modulation. In local power modulation, the feed movement is superimposed by a mostly harmonically oscillating relative movement, whereas in temporal modulation, the energy input varies over the process time. Spatial power modulation has a positive effect on the temperature distribution within the workpiece and welding irregularities, but the welding depth is negatively affected due to the asymmetrical movement. By varying the energy input through temporal power modulation, the asymmetrical energy input can be balanced by adjusting the input energy periodically [13].

Furthermore, the laser wavelength is a key element in laser micro welding and has a decisive influence on the energy coupling into the material to be processed. The absorption of metals such as copper decreases with increasing wavelength. For example, absorption at wavelengths in the blue range is approximately 50%, whereas in the near-infrared range, only approximately 10% absorption can be detected. Aluminum, on the other hand, has the highest absorption around λ = 808 nm [14]. Hummel et al. [15] investigated the effect of wavelengths in the near-infrared and visible wavelength regime on welding for copper. They found out that at higher feed rates (v > 200 mm/s), a 515 nm laser achieves a deeper and more continuous weld penetration but poorer surface roughness due to increased process dynamics.

2.2. Superimposed dual-beam welding

Further investigations combine two laser beam sources. A distinction is commonly made between laser beam welding in parallel arrangement, in tandem arrangement, and coaxial arrangement. Other experimental approaches combine different wavelengths [16]. An overview of different arrangements is shown in **Fig. 1**.

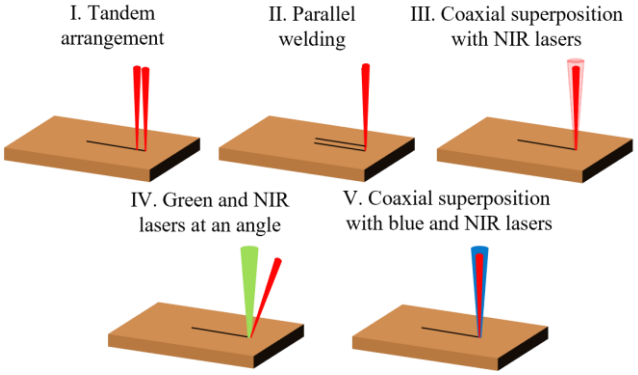

Fig. 1 Arrangements of dual beam superposition: I. Tandem Arrangement [16,17]; II. Parallel welding [16]; III. Coaxial superposition with NIR lasers [18]; IV. Green and NIR lasers at an angle [7]; V. Coaxial superposition with blue and NIR lasers [3]

Even at comparable laser power levels, the resulting weld seam geometry differs significantly depending on the laser wavelength. Blue laser radiation at 445 nm exhibits a

substantially higher initial absorptivity on copper and aluminum surfaces, leading to an earlier onset of melting, a wider melt pool near the surface, and a more homogeneous energy deposition. In contrast, near-infrared radiation at 1070 nm shows a lower initial absorption, resulting in delayed coupling, a narrower seam width, and a stronger dependence on temperature-induced absorption effects. Consequently, at equal laser power, blue and near-infrared laser beams generate fundamentally different weld shapes with respect to seam width, penetration behavior and process stability, noting that beam diameters may also differ in state-of-the-art welding strategies.

When both wavelengths are applied simultaneously in a spatially superimposed dual-beam configuration, the interaction between the lasers is not of optical origin but governed by thermo-physical effects. A blue laser beam locally increases absorption and pre-heats the material surface, thereby enhancing the coupling efficiency of the near-infrared laser. This preconditioning effect stabilizes vapor capillary formation, improves energy deposition and enables a more controlled adjustment of weld seam width and penetration depth.

In tandem laser dual beam welding (I), the vapor capillaries fuse together during the welding process if the distance between the laser spots is kept small enough. Furthermore, the vapor capillary behind the first laser beam has a greater welding depth, which is due to the increased absorption effects caused by the upstream temperature increase. Compared to laser beam welding with a single beam, an improvement in stability can be seen, which is due to a larger melt pool and a larger opening of the vapor capillary [16]. Cui et al. [17] divide a laser with a wavelength of $\lambda = 1070$ nm and a power of 6 kW into two separate beams using an optical prism. The focal points lie on a line in the feed direction. The leading laser heats the material to increase the absorption of the second laser spot and the relative distance of the laser spots influences penetration depth. The seam width and welding depth decrease as the relative position of the spots increases since the heat input of the first laser has no longer a positive effect on the second one.

In parallel laser welding (II), the vapor capillaries merge again if the focal points are close together. If the distance between the individual laser beams is large enough, two separate vapor capillaries with the same welding depth form next to each other. The fusion of both capillaries creates a weld with greater weld penetration depth and a smaller capillary opening [16].

For coaxial superposition (III), Bergman et al. [18] superimpose a diode laser with a wavelength of 808 nm with a solid-state laser of $\lambda = 1064$ nm. A positive effect on crack formation is observed, which is due to a lower cooling rate of the material.

Hess et al. [7] combine a laser with a wavelength of $\lambda = 1030$ nm at an angle of incidence of 18° (IV) and a distance of 100 µm between the focal diameters relative to each other at a wavelength of 515 nm. The laser in the green regime heats the material until it begins to melt and a small vapor capillary is formed. When the NIR laser is additionally activated, the vapor capillary enlarges, and the deep welding process is achieved directly. The combination of the two wavelengths results in a more homogeneous weld seam and reduces the amount of melt ejection. Furthermore, the power of the laser emitting in the near-infrared wavelength range can be reduced to achieve a deep welding process.

For the coaxial superposition of different wavelengths (V), Fujio et al. [3] and Ishige et al. [19] combine a fiber laser of $\lambda = 1070$ nm coaxially with a diode laser that emits a wavelength of $\lambda = 450$ nm. This allows more copper material to be melted and increases process stability. This is due to lower temperature gradients and higher initial absorptions, based on the increased temperature. The penetration depth and uniformity of the penetration depth are improved compared to welding tests with only one near-infrared laser. Furthermore, spatter is avoided during welding because of a larger capillary opening.

2.3. Interim conclusion on the theoretical background

In all the work presented on increasing precision in laser welding, tailored spatial and temporal energy input plays a key role. Particularly with highly reflective materials such as copper, visible wavelengths show potential for positively influencing the welding process through improved energy coupling, but also through relatively large spot diameters with limited welding depth. The following mechanisms and advantages can be noted for the different methods of beam superposition:

- Enlargement of vapor capillary opening for better escape of metal vapor
- Improved energy coupling of the second laser through preheating of the first laser
- Defect reduction through more stable vapor capillaries and lower cooling rates of the material

These aspects are considered in the evaluation of the investigations presented in this paper. As a basis for the further development of compensation methods, multi-wavelength superposition is transferred to laser spots that are offset relative to each other in tandem arrangement.

3. Resources, experimental setup and procedure

The experiments are conducted with two different superimposed beam sources. A diode laser from Laserline GmbH (LDMblue 1800-30) is used for the wavelength of 445 nm and for the NIR-wavelength (1070 nm), a single mode laser from IPG Photonics (YLR-2000-WC) is used. **Table 1** lists some of the technical specifications of the lasers [20,21].

Table 1 Technical specifications of the laser beam sources.

Laser beam source:	Wavelength:	Fiber diameter:	Max. output power	Beam parameter product:
[-]	[nm]	[nm]	[W]	[mm·mrad]
Laserline	445 ± 20	600	1800	33
IPG	1070 ± 5	14	2000	0.37

To ensure that the desired laser power reaches the workpiece, a power measurement was carried out using a "PRIMES cube" with a measuring accuracy of 3% and the target power was calibrated against the actual power. Furthermore, the laser beam caustics of both lasers were determined using the "Focus Monitor FM+" and "MicroSpot-Monitor MSM-35" measuring devices from PRIMES. Based on these measurements, the spot diameter of the blue laser was determined to be 609 µm and of the NIR laser to 34 µm.

The materials analyzed are CuSn6, Cu-ETP and EN AW-6082. The material specific properties are shown in **Table 2**.

Table 2 Material properties of the sample materials

Material:	Density:	Thermal conductivity at 20°C:	Specific heat capacity at 20°C
[-]	[g/cm³]	[W/mK]	[J/kgK]
CuSn6 [22]	8.82	75	3770
Cu-ETP [23	8.93	384	3860
EN AW-6082 [24]	2.7	170-220	8960

CuSn6 is a copper-tin alloy with high strength and good corrosion resistance. It is mainly used in machine and apparatus engineering, specifically where a combination of good strength and electrical conductivity is required. Cu-ETP is an oxygen-containing copper with higher thermal and electrical conductivity than CuSn6 or EN AW-6082. Due to its electrical conductivity, Cu-ETP is primarily used in electronics and electrical engineering. EN AW-6082 is an aluminum alloy that belongs to the group of aluminum-magnesium-silicon alloys. EN AW-6082 has high strength and is used in machine and vehicle construction [22-24]. The materials were chosen to analyze not only different base materials but also the influence of the dual-beam approach on different thermal conductivities and specific heat capacities.

A dual-beam optical system developed in-house is used to merge the two laser beams onto the materials (**Fig. 2**). The beam paths are combined using a dichroic mirror and adjusted relative to each other using moveable lenses that the laser spots have the same focal position. The blue laser spot is always stationary, while the NIR beam can be moved around the blue spot using a galvanometric scanner system. If no offset is used, the two laser spots are located at the same point in x, y and z directions.

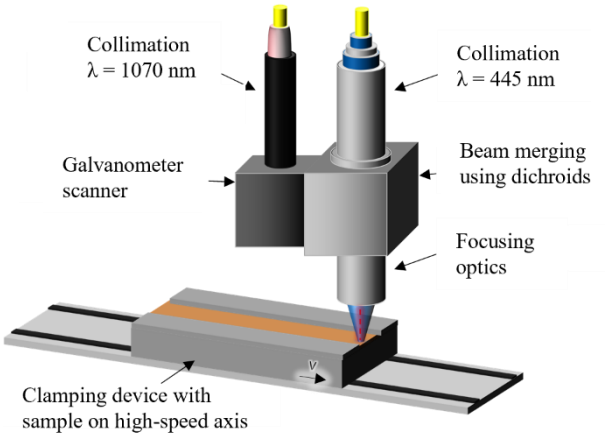

Fig. 2 Schematic experimental setup

The samples are fed by a LINAX Lxs linear motor axis from Jenny Science AG. To protect the focusing optics from possible spatter or smoke residues, a cross-jet which generates an airflow perpendicular to the incident laser beam is used. No protective gas was used in these experiments.

The experiments are performed as blind welds on rectangular samples. The materials have dimensions of 100 × 30 × 2 mm³. To ensure reproducible positioning of the samples, a clamping device with two stops is used. To account for a standard deviation, three welds with a length of 20 mm are performed side by side on one sample. The individual welds are spaced 5 mm apart. In addition, a waiting time of 10 seconds was programmed between the individual welds with the same set of parameters so that the heat input of the individual welds does not influence the subsequent weld. The waiting time is estimated using Newton's cooling law for the three materials and the length of the weld seam. The resulting waiting times are in the range of 10 seconds.

In the first step, at the same feed rate v and with the same distance between the focus points, the laser power of the near-infrared laser varies from 250 W to 750 W in 250 W increments. The power of the blue laser is set to 1000 W and 1500 W respectively. In the next step, three different spot arrangements – downstream, coaxial and upstream (**Fig. 3**) – are analyzed.

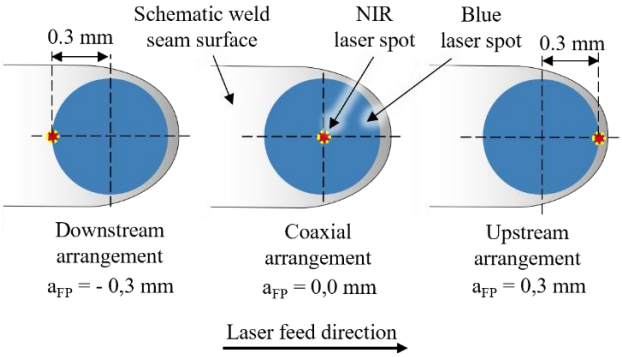

Fig. 3 Comparison of the two spot diameters and visualization of the three spot arrangements: downstream, coaxial and upstream

The weld seam width after solidification is measured using the "Keyence VHX6000" microscope and the roughness by a "Keyence LSM VK-9700" laser scanning microscope. To determine the weld penetration depth, cross sections and longitudinal sections are made from the samples and measured with the VHX6000.

4. Results and discussion

This chapter compares the weld penetration depth d_w, weld seam width w_w and the weld seam roughness Ra for each of the materials. These values are shown on the y-axis and are plotted against the different focus positions arrangements (compare **Fig. 3**).

4.1. CuSn6

Starting with the first graphs, the weld penetration depth d_w is analyzed for CuSn6 in **Fig. 4**.

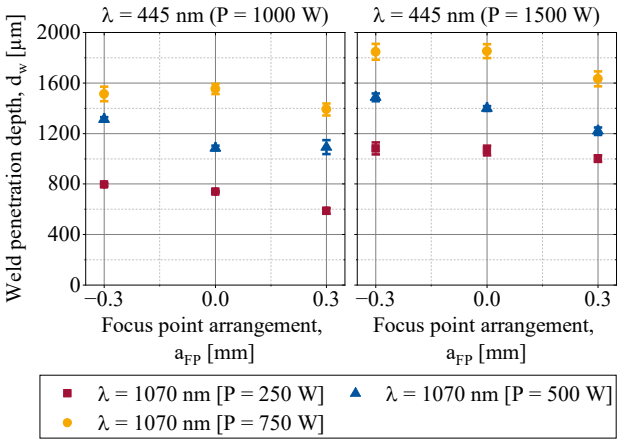

Fig. 4 Weld penetration depth of CuSn6 with v = 100 mm/s

As expected, with increasing laser power of the NIR laser, a significant increase in the welding depth can be identified with a maximum value of 1852 µm in coaxial arrangement and maximum laser powers. In addition, the trend has been identified that an increase in the blue laser power also has an influence on the welding depth. If, for example, the value of coaxial arrangement and a NIR-laser power of 750 W is considered, the welding depth increases by approximately 19% with a 50% (500 W) increase in laser power. The lowest weld penetration depth across all cases can be observed in the upstream (a_{FP} = 0.3 mm) arrangement, with a trend toward increasing weld depth towards the downstream arrangement (a_{FP} = -0.3 mm). To understand the influence of the relative position of the two lasers on the approximate melted volume, the seam width near the surface is examined in **Fig. 5**.

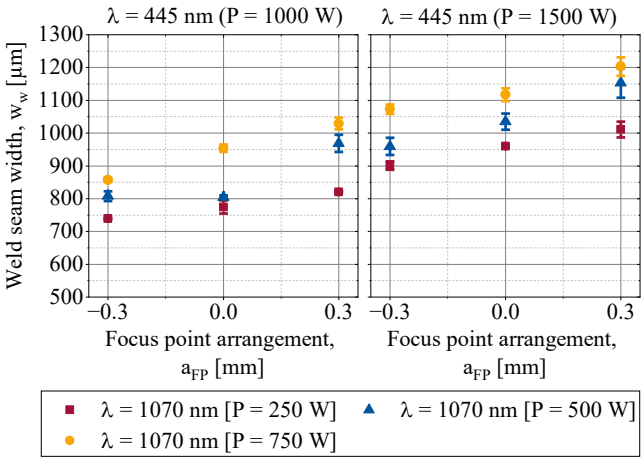

Fig. 5 Weld seam width of CuSn6 with v = 100 mm/s

Looking at both graphs for weld penetration depth (**Fig. 4**) and weld seam width (**Fig. 5**), it is apparent that a change of a_{FP} in the range between -0.3 mm and +0.3 mm fundamentally changes the geometry of the weld seam. If the experiments are conducted in downstream mode, a positive influence on the weld depth is observable, whereas an upstream arrangement has a positive influence on the weld seam width. It is assumed that the molten volume remains approximately constant. This allows to weigh up whether a wider, shallower weld seam or a narrower, deeper one is preferred when determining the parameters. In combination with temporal power modulation, even a variation of these geometric characteristics during the process using a control system may be possible. To explain this phenomenon, the hypothesis proposed is that the upstream blue laser spot opens and stabilizes the vapor capillary and allows the highly focused NIR laser beam to penetrate deeper into the material through multiple reflections. If the blue laser spot is downstream, a wider melt pool is created and the laser radiation from the NIR laser cannot penetrate so deeply because the blue laser does not keep the vapor channel open.

By checking the roughness (**Fig. 6**), no significant increase in surface-related melting dynamics in the form of the surface parameter Ra can be identified.

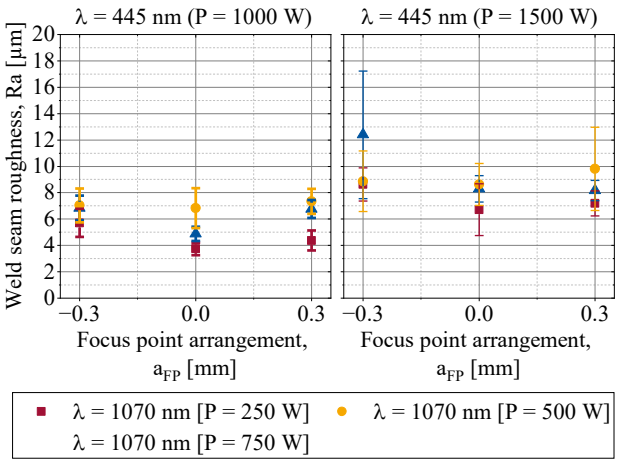

Fig. 6 Weld seam roughness Ra of CuSn6 with v = 100 mm/s

Only by increasing the blue laser power, a minimal increase in the roughness values can be observed which lies within the values for the standard deviation.

4.2. Cu-ETP

For the second material Cu-ETP, the values for the weld penetration depth are shown in **Fig. 7**. With maximum power parameters, a maximum weld penetration depth of 1064 µm can be achieved. Compared to CuSn6, this corresponds to a 57.5% reduction in weld penetration depth, which can be attributed to, among other factors, to the five times greater thermal conductivity (compare **Table 2**).

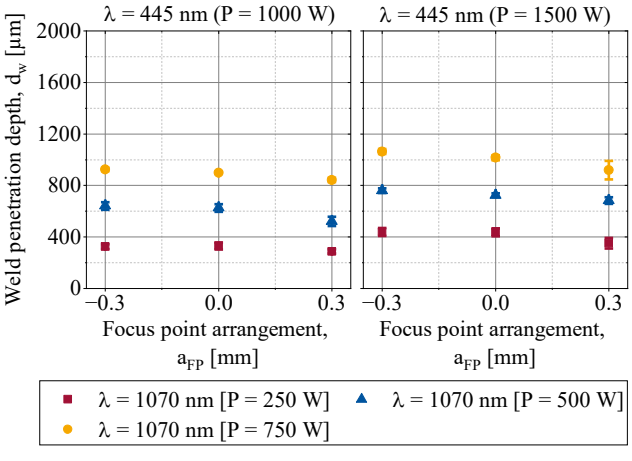

Fig. 7 Weld penetration depth of Cu-ETP with v = 100 mm/s

Similarly, an increase in blue laser power has only a minor influence on the formation of the weld penetration depth. However, a slight trend toward a positive influence on the weld penetration depth can be observed as the red laser is shifted towards a_{FP} = -0.3 mm. Like the weld seam width for CuSn6, the same effect of geometry change can be observed for Cu-ETP (compare **Fig. 8**).

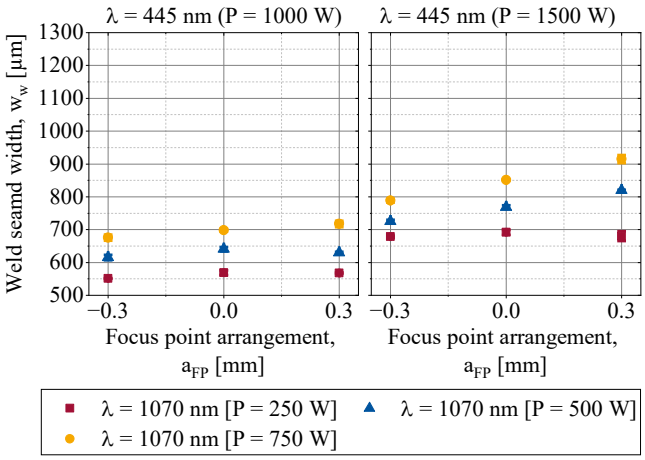

Fig. 8 Weld seam width of Cu-ETP with v = 100 mm/s

Particularly when using the blue maximum laser power of P = 1500 W, a significant increase in weld seam width can be observed from the downstream to the upstream arrangement.

When observing the surface roughness Ra, the values are again similar to CuSn6, so that, taking into account the standard deviation, a value of Ra = 14 µm is not exceeded throughout. However, the standard deviation differs when comparing the materials. Due to the higher thermal conductivity of Cu-ETP and a resulting less dynamic process than with CuSn6, a narrower standard deviation is recorded here.

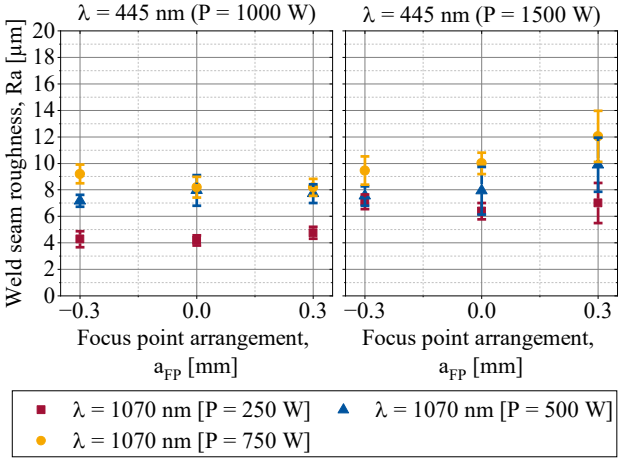

Fig. 9 Weld seam roughness Ra of Cu-ETP with v = 100 mm/s

Yet it should be noted that despite an increase in the weld penetration depth towards the downstream process, the roughness decreases towards the downstream arrangement looking at the higher blue laser power experiments. This is probably due to the fact that in the upstream mode, a rather needle-shaped vapor capillary forms, resulting in a vehemently fluctuating process, while in the downstream mode, the blue laser stabilizes the vapor capillary.

4.3. EN AW-6082

To test another base material in addition to copper for the dual-beam approach, **Fig. 10** shows the weld penetration depth of EN AW-6082.

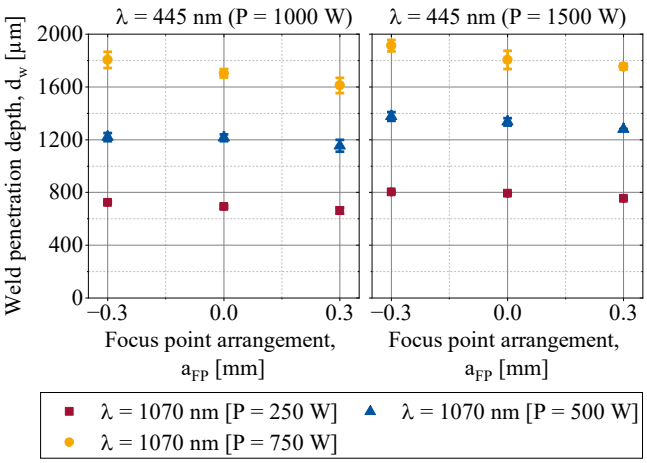

Fig. 10 Weld seam depth of EN AW-6082 with v = 100 mm/s

Although aluminum has a thermal conductivity that lies between the two examined copper materials, at 1913 µm, the highest weld penetration depth is achieved in the downstream arrangement and at maximum laser power parameters considering all experiments in this run. As expected, the blue laser has no longer a significant influence on increasing the welding depth as in copper. Nevertheless, an influence of the upstream arrangement in comparison to the downstream arrangement can be identified, even though this effect is now less apparent.

Regarding the weld seam width (**Fig. 11**), the blue laser at a power of P = 1000 W no longer has any influence on the formation of the weld seam width. The effect of the increase in weld seam width towards the upstream arrangement can be observed with higher laser power of the blue laser.

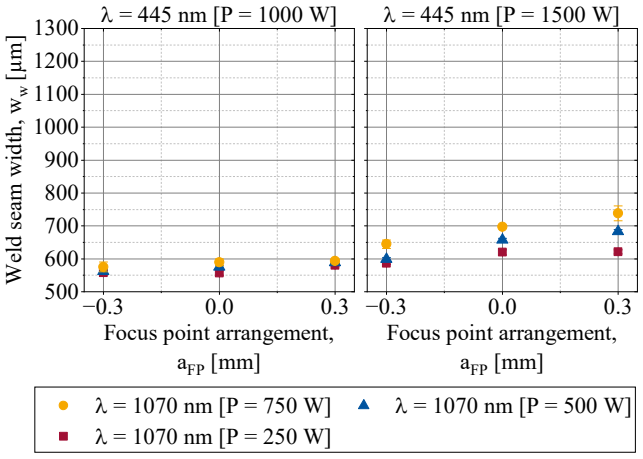

Fig. 11 Weld seam width of EN AW-6082 with v = 100 mm/s

When comparing the roughness, the highest Ra values are achieved in aluminum welds with up to 14.3 µm

excluding standard deviation. An increase in the laser power of both lasers leads to an increase in roughness again.

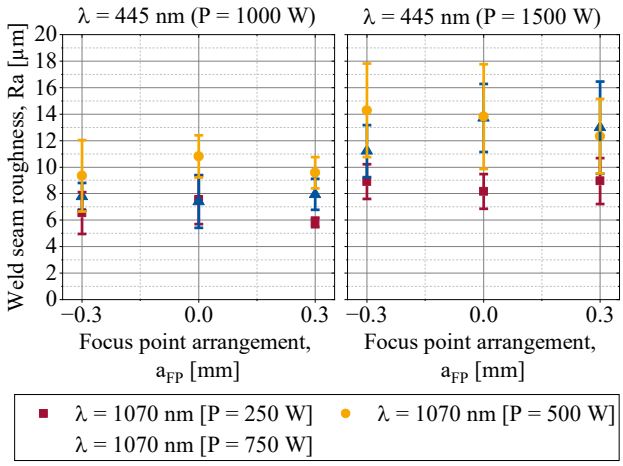

Fig. 12 Weld seam roughness Ra of EN AW-6082 with v = 100 mm/s

Apart from relatively large standard deviations, the data do not allow any meaningful conclusions to be drawn regarding the relative position of the lasers in this case.

4.4. Interim conclusion and material comparison

The experiments have shown that different effects can be observed depending on the material and its specific properties. By shifting the laser spots relative position to each other, it has been shown that greater welding depths can be achieved with a near-infrared laser spot following (downstream arrangement) than with the upstream arrangement. The opposite is true for the weld seam width. Here, the width decreases with the downstream NIR laser spot. If, in turn, the weld penetration depth and weld seam width of the copper basis materials are compared across the three arrangements analyzed, a change in the weld seam geometry can be observed, from a wider, shallow weld seam to a narrower but deeper one. In the area of surface roughness measurement, only limited statements can be made, except for the maximum and minimum values that can be achieved. Among a variety of process influences, this is since the flaking of the different materials develops differently under the same parameters (compare **Fig. 13**).

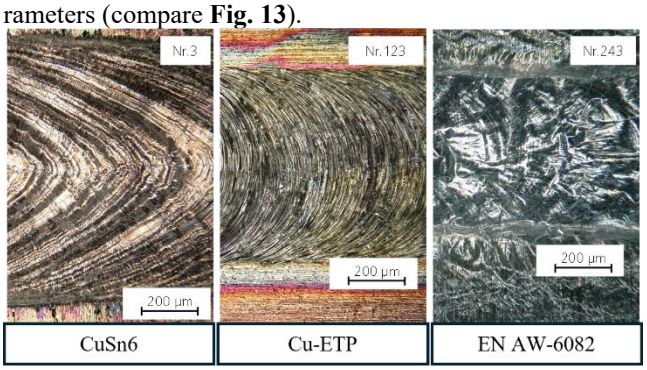

Fig. 13 Surface images of CuSn6, Cu-ETP and EN AW-6082 at P(445 nm) = 1000 W, P(1070 nm) = 750 W, v = 100 mm/s, a_{FP} = 0 mm

The surface images in **Fig. 13** of the three materials show that the weld seam bead develops differently due to the dynamics and geometry of the melt pool and the solidification behavior. Whereas a V-shaped flaking occurs at a feed rate of 100 mm/s with CuSn6. If the cross sections are viewed considering the same parameters (**Fig. 14**), it can also be seen that when the two laser beams are superimposed, different geometries form in the depth of the material. Whereas CuSn6 forms a homogeneous V-shaped weld seam cross section, the solidified melt in Cu-ETP looks like a thumbtack. Aluminum takes on a form that is somewhere between the two extremes.

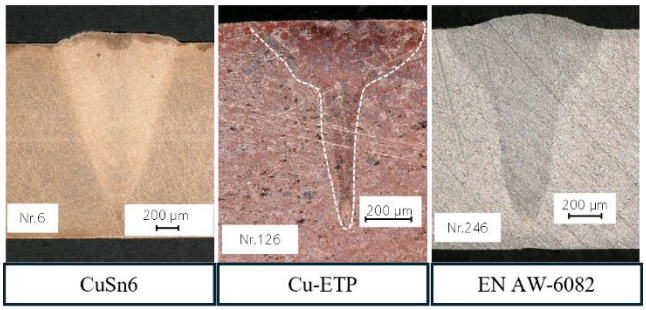

Fig. 14 Cross section images of CuSn6, Cu-ETP and EN AW-6082 at at P(445 nm) = 1500 W, P(1070 nm) = 750 W, v = 100 mm/s, a_{FP} = 0 mm

The results and weld seam images show that laser beam superimposition creates new degrees of freedom for producing customized geometries, which can also be modified during the process by superimposed temporal power modulation.

5. Conclusion

In the scope of this paper, a dual-beam approach was presented in which a static blue laser spot with λ = 445 nm is superimposed with a dynamically modulated near-infrared laser beam source (λ = 1070 nm). In addition to varying the laser parameters, the relative position of the laser spots was changed so that the near-infrared laser beam could be examined upstream, coaxially or downstream to the blue laser spot. In summary, the following statements can be made:

- When welding copper in dual-beam welding, both the blue and NIR laser have a significant influence on the weld penetration depth.
- If the near-infrared laser spot is positioned downstream of the blue laser spot, the weld penetration depth increases.
- Conversely, the weld seam width decreases when the NIR laser is downstream positioned.
- The maximum measured roughness's values Ra are less than 14 µm for copper and less than 20 µm for aluminum.

Based on the results, the conclusion can be drawn that superimposing laser beams using a multi-wavelength approach can improve the precision of a laser weld regarding weld seam width, surface roughness, weld penetration depth and weld depth consistency, when the relative positions of the beams are adjusted accordingly. These findings are directly applicable to EV battery tab welding and electronic interconnects, where high penetration with low spatter and consistent seam geometry are critical for electrical performance and manufacturing throughput. With suitable adjustment of the parameters of the two laser beam sources, dual-beam laser

welding can produce application-adapted tailored weld seam geometries.

Acknowledgment
The experimental setup and its operation were funded by the Deutsche Forschungsgemeinschaft e.V. (DFG, German Research Foundation) within the framework of the Collaborative Research Centre SFB1120-236616214 "Bauteilpräzision durch Beherrschung von Schmelze und Erstarrung in Produktionsprozessen".

Data Availability Statement
The data that supports the findings in this study are available upon reasonable request. Selected data are available after authorization in Coscine with the persistent identifier (PID) http://hdl.handle.net/21.11102/73ce8c3e-aa64-4c57-afb0-56bcafc650e5 (accessed on June 26, 2025). For further information, please contact the corresponding author.

References

[1] C. Hoff, N. Otero, J. Hermsdorf, S. Kaierle, and L. Overmeyer: Metall, (2015) 439.
[2] M. Hagedorn, S. Hartmann, D. Heilert, C. Harter, I. Olschwewski, L. Eckstein, M. Baum, T. Henzelmann, and T. Schlick: Automobile Wertschöpfung 2030/2050: Studie im Auftrag des Bundesministeriums für Wirtschaft und Energie (2020), 4.
[3] S. Fujio, Y. Sato, K. Takenaka, R. Ito, M. Ito, M. Harada, T. Nishikawa, T. Suga, and M. Tsukamoto: J. Laser Appl., (2021) 042056.
[4] V. Mann, F. Hugger, S. Roth, and M. Schmidt: Applied Mechanics and Materials, (2014) 89.
[5] F. Kaufmann, A. Meier, J. Ermer, S. Roth, and M. Schmidt: Laser in Manufacturing Conference (2021)
[6] H. Hügel and T. Graf: Materialbearbeitung mit Laser: Grundlagen und Verfahren (Springer Vieweg, Wiesbaden, 2023) 142.
[7] A. Hess, R. Schuster, A. Heider, R. Weber, and T. Graf: Physics Proc., Part A, (2011), 88.
[8] S. Hollatz: Funktionsorientiertes Laserstrahl-Mikroschweißen von Aluminium-Kupfer-Verbindungen mit örtlicher Leistungsmodulation (Apprimus Verlag, Aachen, 2023) 7.
[9] A. Hess: Vorteile und Herausforderungen beim Laserstrahlschweißen mit Strahlquellen höchster Fokussierbarkeit (Utz Verlag, Stuttgart, 2012), 12.
[10] R. Poprawe: Lasertechnik für die Fertigung: Grundlagen, Perspektiven und Beispiele für den innovativen Ingenieur (Springer Berlin, Heidelberg, 2005) 257.
[11] M. Hummel, C. Meier, A. Olowinsky, A. Gillner, F. Beckmann, J. Moosmann, and C. Häfner: J. Manuf. Mater. Process, (2024) 47.
[12] F. Schmitt: Laserstrahl-Mikroschweißen mit Strahlquellen hoher Brillanz (Shaker Verlag, Aachen, 2012) 20.
[13] A. Häusler: Präzisionserhöhung beim Laserstrahl-Mikroschweißen durch angepasstes Energiemanagement (Apprimus Verlag, Aachen, 2021) 21.
[14] J. G. M. Helm: Prozessstabilität und Prozesseffizienz beim Laserstrahlfügen von hoch reflektiven Kupferwerkstoffen (Apprimus Verlag, Aachen, 2022) 13.
[15] M. Hummel, C. Meier, A. Olowinsky, A. Gillner, F. Beckmann, J. Moosmann, and C. Häfner: Proc. SPIE, Vol. 12414, (2024) 124140A.
[16] S. Gong, S. Pang, H. Wang, and L. Zhang: Schweißbad-Dynamik beim Laser-Tiefschweißen (Springer Nature, Singapore, 2024) 200.
[17] L. Cui, B. Chen, S. Nai Mui Ling, and J. Wei: Journal of Materials Processing Technology, (2015) 287.
[18] J. P. Bergmann, M. Bielenin, M. Stambke, T. Feustel, P. Witzendorf, and J. Hermsdorf: Physics Procedia, (2013) 180.
[19] Y. Ishige, H. Hashimoto, N. Hayamizu, N. Matsumoto, and F. Nishino: Proc. SPIE, Vol. 11668, (2021) 116680M.
[20] Laserline GmbH: LDMblue 1800-30: User manual diode laser, 2022.
[21] IPG Photonics: User manual, IPG Laser, YLR-2000-WC, 2019.
[22] Deutsches Kupferinstitut: CuSn6, 2005.
[23] Deutsches Kupferinstitit: Cu-ETP, 2005.
[24] ALUMERO: AW-6082, 2018.

(Received: June 30, 2025, Accepted: January 14, 2026)